Mustansiria Dental Journal
MDJ

Vol.21, No.02, 12/2025
P- ISSN: 1813-8500
E- ISSN: 2618-0944

Impact of Different Fiber Reinforcement Techniques on Stress Distribution of Cervical Composite Restorations: Finite Element Analysis.

Ali Nahidh[1], Abdallah Ahmed Elsherbiny[2], and Ahmed Sleibi[3]

[1]Department of Conservative Dentistry, College of Dentistry, Mustansiriyah University, Baghdad, Iraq. E-mail: alinihdh970@gmail.com. ORCID: https://orcid.org/0009-0005-3896-6657.

[2]Production Engineering and Mechanical Design Department, Faculty of Engineering, Mansoura University, Mansoura, Egypt. E-mail: abdalla.a.m@mans.edu.eg.

[3]Department of Conservative dentistry College of Dentistry, Mustansiriyah University, Baghdad, Iraq. E-mail: sleibi1975@uomustansiriyah.edu.iq, ORCID ID: https://orcid.org/0000-0002-7747-7785 .

Received 21/07/2025 ***Accepted in revised form 15/12/2025*** ***Published 30/12/2025***

Abstract

Aim: To compare the stress distributions in the cervical cavities of four different restorations using Von Mises stress under varying loading directions. **Methods:** Virtually restored lower first premolar models (n=4) with class V cavities were created from a sound premolar CAD model. Single restorative materials of a resin-modified GIC (model A), a conventional filler composite (CFC) (model B), a combination of short-fiber-reinforced composite-CFC (model C), and a ribbond fiber-CFC (model D) in a bilayered fasion were considered in this study. The FEA models received a 150 N occlusal load in the axial and oblique directions. The stress distribution in the enamel and dentin components of the model and restorative sections was analysed. The maximum von Mises criterion was determined and compared between the tested models. **Results:** The FEA model indicated that the highest mvM was detected in the enamel structure of the premolar. Notably, greater stresses were observed in the GIC (Model A) and CFC (Model B) restorations than in the combined EverX-CFC restoration (Model C), which resulted in less stress in the enamel and dentin. Finally, the bilayered ribbond-CFC restoration (Model D) had the lowest stress values among the different components of the model. In the oblique loading scenario, all the models with various components presented higher stress values than did those with axial loading, with slightly lower stress values in the fiber-reinforced composite restorations. **Conclusion:** The incorporation of either glass or polyethylene fibers within the cervical composite restoration apparently enhances stress distributions on the surrounding tooth structure, thus probably improves the retention rate of the restoration.

Keywords: Finite element analysis, short fiber reinforced composite, Ribbond fibers, cervical cavity, Resin modified GIC.

1. Introduction:

The restoration of cervical lesions, encompassing both carious and noncarious defects, is a unique clinical situation. The longevity and retention of these cavities are a day-to-day challenge for dentists. The restoration of cervical lesions is challenging because of their poor retentive cavity shape and cervical edges situated on dentin or cementum, which are detrimental to resin bonding **(Kubo et al., 2006)**. The retention rates of restorative materials are substantially influenced by continuous occlusal loading and their mechanical qualities **(Jordehi et al., 2019)**.

Biomechanical theory posits that cuspal flexure induces mechanical overload of cervical enamel, resulting in tensile and shear stress in the tooth's cervical region, hence affecting the durability of restorations **(Yazici et al., 2003)**. Adhesive materials, such as resin composites and glass ionomer cements, are indicated to replace the lost tissue in the cervix **(Fagundes et al., 2014)**. The conventional resin composite is currently the most widely used direct restorative material because of its many physiomechanical properties **(Leprince et al., 2014)**.

The incorporation of fibers into conventional filler composites (CFCs) constituted one of the most effective enhancements. Glass and polyethylene fibers are the most often utilized types of fibers in dentistry. In 2013, a short fiber-reinforced composite (SFRC Tokyo, Japan, introduced X Posterior) was introduced and designed to mimic the stress-absorbing properties of dentine **(Lassila et al., 2016, Safwat et al., 2021)**

On the other hand, fibers composed of leno wave ultrahigh-molecular-weight polyethylene (LWUHMWPE) serve as alternative reinforcement adhesive materials. The design of the fibers is based on locked nodal crossings and multidirectional yarns, which generate numerous load channels and disperse occlusal loads over a broader area of dental restoration. The integration of polyethylene fibers in the occlusal area of a dental restoration significantly enhances its fracture resistance **(Agrawal, 2014, Zotti et al., 2023a)**.

Several studies have demonstrated how these fibers are essential for enhancing the toughness of composite restorations, reducing the effects of polymerization shrinkage stress, increasing the stress distribution at the tooth-restoration interface, and increasing the favorable mode of failure **(Garoushi et al., 2013, Lassila et al., 2016, Lassila et al., 2018, Khan et al., 2023)**. However, there is a lack of clear evidence regarding the beneficial effect of using fiber-reinforced composite restorations in cervical cavities, particularly extensive ones, and how they can affect the distribution/transfer of occlusal stress. The cervical cavities biomechanically differ from the other cavities regarding the direction of the forces **(Ispas et al., 2019)**. Inspite of the truth that the cervical restorations are not subjected directly to the occlusal forces unlike occlusal restorations, that in turn gives an impression to many dentists to be less catious and precise in selecting the appropriate restorative materials in the cervical region, unfortunately, the cervical

region is subjected to subject to lateral, shear, and flexural stresses that put a high dislodging forces on the cervical restorations **(Machado et al., 2017)**. The incorporation of the fibers within cervical cavities could be beneficial to distribute these stresses, which might affect the longevity of the cervical restorations.

Finite element analysis (FEA) is currently a prevalent research methodology in the biomedical sciences owing to its accuracy and diverse ability to calculate stress and strain in complex three-dimensional (3D) biomedical models **(Soares et al., 2008)**. In dentistry, most structures are dynamically influenced by occlusal force, and FEA has already proven to be useful for assessing the stress distribution of restorative materials **(Ausiello et al., 2017)**. FEA studies have shown the correlation between the mechanical properties of restorative materials and the patterns, number of stresses in the restored cervical area. A more deformation of the interfacial cervical gap occurred with the lower restorative material elastic modulus **(Hollanders et al., 2020)**. Composite resin, with the current adhesive strategies, presented good stress distribution in the cervical area and a lower risk of bonding failure **(Luo et al., 2022).** The aim of this FEA study was to determine the effect of fiber incorporation within cervical restorations and how these fibers influence the stress distribution in the cervical areas. The potential effects of different loads on the stress distribution are analyzed for four different materials: conventional filler composite (CFC), combined SFRC-(CFC), combined Ribbond-CFC, and resin-modified glass ionomer restorative material (RM-GIC).

2. Methodology

1.1. Generation of a solid model:

The 3D tooth model was obtained by scanning an intact lower first premolar, which was extracted for orthodontic reasons, via cone beam computed tomography (CBCT) (Planmeca ProMax 3D Mid machine; Helsinki, Finland). This was done to obtain accurate geometry and dimensions of the tooth (Fig. 1a).

A reverse engineering program known as 3D slicer (open-source software, https://www.slicer.org) was subsequently employed to convert the scanned data into a comprehensive CAD 3D model (Fig. 1b). The preceding established two corresponding structures, one representing the enamel and the other the dentine, both of which were in continuous contact over the entire dentinoenamel junction. The pulp space was represented as a void within the dentine volume due to its Young's modulus being insignificantly tiny in comparison to that of the adjacent enamel and dentine **(Ichim et al., 2007a)**. The STL files were then imported into SolidWorks 2014 software (Dassault Systémés SolidWorks, Waltham, MA, USA). For designing the cervical cavity and different restorative materials that were applied in this study.

A kidney-shaped cavity was modeled on the buccal cervical third of the premolar measuring 5 mm mesiodistally, 3 mm occlusogingivally and 2 mm deep, with the gingival cavity margin located 0.5 mm above the CEJ, as shown in Figure 2. The restored models were derived by Boolean procedures (in SpaceClaim) between the cavity, enamel, and dentin surfaces.

The four models were generated according to the four restorative materials:

I. Model A: This model represents glass ionomer restorative material (GIC, Fuji II, GC Corp., Tokyo, Japan), where the cavity is filled with the GIC.

II. Model B: the cavity was filled with a conventional filler composite (3M, Z350, Oral Care, St Paul, MN, USA). The internal and external cavity walls were covered with a 50 μm adhesive layer.

III. Model C: the cavity was restored with outer and inner restorative layers in a bilayered fashion. The inner layer represents the fiber reinforcement, which here is the everX composite (everX Posterior from GC, Tokyo, Japan) modeled as a 1 mm thick inner layer, whereas the outer layer is filled with a conventional composite (combined SRFC-CFC), as illustrated in Figure 2.

IV. Model D: The cavity was also restored in a bilayered fashion, with a 1 mm inner polyethylene fiber reinforcement layer (ribbond fibers+ flowable composite+ adhesive layer) (Ribbond Inc., Seattle, WA, USA). This was covered with a 1 mm conventional filler composite as an outer restorative layer, which filled the rest of the cavity (combined Ribbond-CFC). This is illustrated in Figure 2 and Table 1.

The above models were embedded in a rectangular block representing the supporting bone volume with a 0.3 mm shell around the tooth root simulating the periodontal ligament (Ichim, Kuzmanovic, and Love 2006).

1.2. Numerical simulation

The mechanical properties of the four restored models (Table 1) were examined using 3D finite element analysis conducted with Abaqus, 19 packages (fllibbit, Karlsson, and Sorensen, Inc., Providence, RI). The components of the models were meshed using Abaqus 2019 software. All volumes were discretised using the 4-node tetrahedral element CTETRA, with a global size varying from 0.05 mm to 0.15 mm. Mesh refinement techniques were employed to reduce the dependency of outcomes on mesh size, due to the tiny radius of curvature and notch effects. Each geometric model underwent meshing, yielding a total of 191,475 nodes and 933,527 elements in the complete assembly.

A mesh quality assessment confirmed the structural integrity of the mesh. Key metrics include a shape factor of 0.846, demonstrating balanced element geometry, and angular bounds of 38.66°–79.55°, ensuring stability and mitigating distortion risks. The mean aspect ratio of 2.43 supports numerical precision, while a geometric deviation factor of 2.53×10^{-5} reflects exceptional geometric fidelity. A stable time increment of 3.15×10^{-6} sec guarantees robust transient analysis, and edge-length ratios (0.149/0.255) validate uniform discretization. All diagnostic checks were passed, with warnings confined to 0.005–0.03% and zero critical errors (Fig. 3), affirming negligible numerical artifacts. To optimize computational efficiency, a mesh sensitivity study was performed, evaluating stress convergence across element sizes (0.04 mm to 0.008 mm). Results (Table 2) show progressive stress stabilization (12.58 MPa → 19.83 MPa) (the representative model here was Model A in Fig. 6a), confirming mesh independence at finer resolutions. This rigorous validation ensures both accuracy and cost-effectiveness in subsequent simulations.

Boundary conditions are essential in finite element analysis since they delineate node displacements and interrelations **(Elraggal et al., 2024)**. All models adhered to the following conditions:

(1) All materials in the models were homogeneous, isotropic, and demonstrated linear elasticity.

(2) FEA models were securely anchored into the alveolar bone and constrained from movement (0° freedom in all directions) to avert any rigid body motion.

(3) Boundary conditions were uniformly implemented across nodes, guaranteeing the absence of defects in any finite element analysis.

The material properties of all the components of the FEA model are presented in Table 3. Static loading of the models (150 N) was applied on the buccal and lingual cusp tips in the axial direction, and the same amount of load was used in an oblique manner on the lingual incline of the buccal cusp to simulate occlusal interference **(Machado et al., 2017)**. A concentrated type of force was also used to generate greater tensile stresses around the cervical region **(Rees and Jacobsen, 1998)**. The load directions and locations are shown in Figure 4. Each model subjected to two times loading, once in axial direction and once in oblique one with the same amount of load. The stress patterns for several models were computed using computer-aided software (Abaqus, 19 packages). The assessment encompassed the analysis of the maximum von Mises (mvM) stresses on the enamel, dentine, fiber-reinforced composite, conventional filler composite, and GIC measured in megapascals (MPa).

The numerical data produced by the FEA is graphically depicted in colour, with analogous colours signifying comparable stress distribution ranges; red areas indicate the highest stress concentrations, while blue areas reflect lesser stresses. Each element of the FEA was isolated and analysed to investigate the stress distributions within the separate components of the models. **(Elraggal et al., 2024).**

3. Results:

Quantitative statistics concerning mvM for various model components are shown in Table 4 (axial loading) and Table 5 (oblique loading). The results are also depicted as bar charts in Fig. 5a-b. Figures 6–7 illustrate the stress distributions across different components of the FEA model. The colour range from red (denoting the highest stress concentration) to blue (showing lower stress levels) illustrates the stress gradients throughout these parts.

In general, the maximum mvM was detected in the enamel structure of the premolar within the FEA model. Notably, higher stresses were observed in Model A and Model B than in Model C, which presented less stress in both enamel and dentin. Model D presented the lowest stress values among the different components of the model during axial loading. In the case of oblique loading, all the models with various components presented higher stress values than did those with axial loading, with slightly lower stress values in the fiber-reinforced composite restorations.

3.1. Stress distribution during axial loading.

3.1.1 Stress distribution in GIC restoration and tooth substrates in the case of axial loading (Model A)

In the mvM distribution of GIC shown in Fig. 6 **a-c**, the FEA revealed zones of maximum stress concentration at the outer tooth substrate (enamel), intuitively at the initial load site and at the axial and axiodistal line angles around the tooth-restoration interface, in addition to the cervical region underneath the restoration. The stress levels ranged from high values (19.8 MPa) (red areas) to low values (blue areas), as shown in Fig. 6**a**.

The restorative component of the model has relatively lower stress values, which peak at 0.94 MPa, with obvious areas of stress concentration at the occlusal part of the restoration (Fig. 6**b)**.

Compared with the enamel layer, the inner tooth substrate (dentin) has relatively lower stress values, with a peak level of 2.45 MPa, and is particularly concentrated at the axial wall of the cavity (Fig. 6**c)**.

3.1.2. Stress distribution in conventional composite restoration and tooth structures (Model B).

The von Mises stress distributions in the conventional composite restoration and surrounding tooth structures are illustrated in Fig. 6**d-f**. The enamel component reveals high stress values, mainly at tooth restoration interfaces in the cervical area, with a marked stress concentration at the mesioaxial and distoaxial tooth extremities, with a peak value of 13.3 MPa, which decreases to much lower values at other parts of the enamel until zero (Fig. 6**d)**. The dentine component has much lower stress values than the enamel substrate does (1.64 MPa) (Fig. 6**f)**. Compared with the enamel and dentin, the restorative part presented lower stress values (0.66 MPa), as illustrated in Fig. 6**e**. These stresses are concentrated mainly at the occlusal surface of the restoration.

3.1.3. Stress distribution in the Ever X-CFC bilayered restoration and surrounding tooth structures (Model C).

The von Mises stress distributions for the Ever x-CFC combination are illustrated in Fig. 6**g-i.** Relatively low stress values are shown for the enamel component, with a peak value (9.48 MPa) at 9.5 **g**. The dentinal substrate has very low stress values, which peak at 0.92 MPa (Fig. 6**i)**. The restorative part, which is represented by the inner FRC layer and outer CFC layer, reveals a characteristic stress distribution where the outer layer shows relatively marked stress concentration in multiple areas, particularly near the interfaces, whereas the inner layer, in comparison with the outer layer, clearly has lower stress values, as shown in Fig. 6**h**, with the whole restorative part having stress values that peak at 0.24 MPa.

3.1.4. Stress distribution in Ribbond-CFC bilayered restoration and tooth substrates (Model D).

The von Mises stress for this model is illustrated in Fig. 6**j-l**. The stresses are mainly concentrated in the cervical area at tooth restoration interfaces, with a tendency to be particularly directed toward the tooth extremities both mesially and distally, in the outer enamel structure. In this case, the enamel layer also had relatively greater stress values than both the dentinal and restorative components, which peaked at 6.31 MPa (Fig. 6**j)**. However, the dentin part presented a lower value, which reached a maximum value of 0.57 MPa (Fig. 6**l)**. The multilayered restoration here shows a variable stress distribution where the inner ribbond layer has lower stress values than the outer CFC layer, with a peak value for the whole restoration, which reaches 0.19 MPa (Fig. 6**k)**.

3.2. Stress distribution during oblique loading:

All FEA models with different restorative materials revealed an increase in von Mises stress during oblique loading. In general, all the models with different restorative options presented increased stress values during oblique loading, as illustrated in Table 5 and Fig. 5b. Model A presented the highest stress values among the other models, followed by Model B, which presented lower stress values for the different model components. Models C and D clearly presented minimal stresses compared with Model D, which presented the lowest stress values with respect to the other models.

The pattern of the stress is approximately the same as that in the state of axial loading, where high stresses are concentrated at the tooth-restoration interfaces, particularly at the axial and distoaxial line angles. The cervical region also shows areas of increased stress in all the models, which is obviously greater than that at the occlusal part of the restorations in the vicinity of the tooth. Model C and Model D yield minimal von Mises values in all the parts of the model, with the exception of the restorative component of Model D, where a relatively high stress value is observed, whereas both tooth substrates have the lowest value among the other models. The von Mises stresses for all the models in the case of oblique loading are shown in Fig. 7**a-l.**

4. Discussion:

This study used 3D finite element analysis to examine the effects of both short- and long-fiber reinforcements on the biomechanical response of direct restorative strategies for cervical defects when an occlusal load is applied.

Four 3D models have been designed to compare the materials routinely used to restore cervical lesions **(Ichim et al., 2007b, Narayanaswamy et al., 2008, Bezerra et al., 2020, Schwendicke et al., 2021),** represented by conventional filler composites, GICs, and fiber-reinforced composites (FRCs), which have been sufficiently investigated in different modalities **(Garoushi et al., 2018, Lassila et al., 2018, Lassila et al., 2020, Escobar et al., 2023)**.

This analysis enables the assessment of how these fibers influence the biomechanics of the restored cervical region, aiming to achieve optimal stress distribution, minimize fracture risk, and prolong the durability of cervical restorations. The premise behind this approach is that restoring the cervical cavities with conventional composite resin, which is currently the most commonly used material for cervical restoration, would be less than ideal; instead, reinforcing it with a laminate of short fibers (SFRC) or long polyethylene fibers (ribbonds) would be more advantageous for resisting the stresses of functional and parafunctional occlusal loading, particularly in extensive cavities and in noncarious cervical lesions (abfraction cases), where high mechanical demands for restorative materials need to be considered **(Hollanders et al., 2020, Jakupović et al., 2022).**

This study demonstrated that the differing stress concentrations in various restorative materials are predominantly affected by their modulus of elasticity and Poisson's ratio under analytical settings. Our findings revealed adverse effects with GIC restoration (Model A), where high von Mises stress concentrations were exhibited through the tooth substrates and the restorative component (axial load; 19.8

MPa in enamel, 2.45 MPa in dentin, and 0.92 MPa in the restorative part). In the case of the oblique load, higher stresses are concentrated in the cervical region, which is consistent with previous studies **(Ichim et al., 2007b, Machado et al., 2017).** This is illustrated in Tables 4--5 and Figures 6.a--c. and Fig. 7.a--c. The above results might be attributed to the low elastic modulus of GIC (8 MPa), permitting the material to deform under the occlusal load, thereby transmitting the stresses to the underlying tooth structures. This phenomenon may result in marginal breakdown at the tooth-restoration interface and eventually adhesive or cohesive restoration failure **(Yamanel et al., 2009, Hasija et al., 2014).**

Compared with GIC restoration, composite resin restoration as a single restorative material represented by model B (CFC), revealed lower von Mises stresses under both types of loading (axial and oblique). This finding is consistent with previous studies that demonstrated the preeminence of cervical composite restorations in terms of stress distribution and marginal stability **(Hasija et al., 2014, Dikova et al., 2020, Dikova et al., 2021).** However, Model C and Model D represent the bilayered fasion of the cervical composite restoration, where a layer of fiber reinforcement placed as a substructure underneath the conventional composite resin (CFC) characteristically showed minimal stress values.

In Model C, a layer of short fiber-reinforced composite beneath the conventional composite indicatively reduced the stresses during both types of loading, where under axial loading, the von Mises values were 9.5 MPa in the enamel, 0.92 MPa in the dentin and 0.24 MPa in the restorative component, whereas under oblique loading, the stress values were 9.53 MPa, 1.36 MPa, and 1.77 MPa in the enamel, dentin and restoration, respectively.

In the literature, the reinforcement of composites with short fibers as a dentin replacement material had positive effects on the biomechanical behavior of the final composite restorations. This occurs through enhancing the stress distribution, increasing the fracture resistance of the composite resin in response to various occlusal loads **(Garoushi et al., 2018, Soares et al., 2018, Suzaki et al., 2020, Barreto et al., 2016).**

In Model D, a laminate of the ribbond fibers is placed upon the axial wall of the cervical cavity and then covered with a CFC layer in a manner that is known clinically as a wallpaper technique **(Deliperi et al., 2017)**. This multilayered composite restoration has been proven in other cavity designs and scenarios to serve well in terms of enhancing the composite biomechanics, distributing stresses, and absorbing the energy of the applied occlusal loads, with a trend to be used, particularly in extensive cavities **(Mangoush et al., 2021, Zotti et al., 2023b, Zotti et al., 2024).** In a different study, these fibers, even when used as intracanal posts in some cases, provided favorable stress distributions in the cervical region (Jain et al., 2024).

Model D reveals the lowest stress values among the other models under axial loading and oblique loading, whereas under axial loading, the von Mises stresses are the minimal stresses compared with those of models A, B and C (6.3 MPa, 0.57 MPa and 0.19 MPa in the enamel, dentin, and restorative components, respectively). Under nonaxial loading, the values are the lowest, with the exception of the restorative part, which has a relatively increased stress value due to the high elastic modulus of the

ribbond layer; however, in the tooth substrates, the stresses are the lowest. The results indicate that materials with a relatively high elastic modulus can reduce the stresses in the surrounding tooth substrates, which is in accordance with previous studies **(Asmussen and Peutzfeldt, 2008) (Kim et al., 2021)**.

The limitations of this study include the following: first, all the materials within the models are uniform and isotropic, exhibiting linear elasticity; second, the acting force is assumed to be static rather than dynamic, as is realistic. Well-standardized in vitro and in vivo studies need to be conducted to confirm the results of this study.

5. Conclusion:

The incorporation of either glass or polyethylene fibers within the cervical composite restoration apparently enhances stress distributions on the surrounding tooth structure, thus probably improves the retention rate of the restoration.

Conflict of interest

The authors declare that there are no conflicts of interest regarding the publication of this manuscript.

Acknowledgments

The authors would like to thank Mustansiriyah University (www.uomustansiriyah.edu.iq), Baghdad, Iraq, for their support in the present work.

Funding: This study is part of MSc project and is partially self-funded.

Ethics approval and consent to participate

This study was approved by the Ethics Committee of the College of Dentistry, Mustansiriyah University (approval no. MUOPR29). Informed consent from the subject (adult orthodontic patient) was obtained prior to the tooth extraction.

References:

1- AGRAWAL, M. J. J. A. M. D. S. R. 2014. Applications of ultrahigh molecular weight polyethylene fibres in dentistry: A review article. 2**,** 95-99.

2- ASMUSSEN, E., PEUTZFELDT, A. & SAHAFI, A. J. T. J. O. P. D. 2005. Finite element analysis of stresses in endodontically treated, dowel-restored teeth. 94**,** 321-329.

3- ASMUSSEN, E. & PEUTZFELDT, A. J. D. M. 2008. Class I and Class II restorations of resin composite: an FE analysis of the influence of modulus of elasticity on stresses generated by occlusal loading. 24**,** 600-605.

4- AUSIELLO, P., CIARAMELLA, S., DI RIENZO, A., LANZOTTI, A., VENTRE, M. & WATTS, D. C. J. D. M. 2019. Adhesive class I restorations in sound molar teeth incorporating combined resin-composite and glass ionomer materials: CAD-FE modeling and analysis. 35**,** 1514-1522.

5- AUSIELLO, P., CIARAMELLA, S., MARTORELLI, M., LANZOTTI, A., ZARONE, F., WATTS, D. C. & GLORIA, A. J. D. M. 2017. Mechanical behavior of endodontically restored canine teeth: Effects of ferrule, post material and shape. 33**,** 1466-1472.

6- BARRETO, B. C. F., VAN ENDE, A., LISE, D. P., NORITOMI, P. Y., JAECQUES, S., SLOTEN, J. V., DE MUNCK, J. & VAN MEERBEEK, B. J. C. O. I. 2016. S hort fibre-reinforced composite for extensive direct restorations: a laboratory and computational assessment. 20**,** 959-966.

7- BEZERRA, I. M., BRITO, A. C. M., DE SOUSA, S. A., SANTIAGO, B. M., CAVALCANTI, Y. W. & DE ALMEIDA, L. D. F. D. J. H. 2020. Glass ionomer cements compared with composite resin in restoration of noncarious cervical lesions: A systematic review and meta-analysis. 6.

8- DELIPERI, S., ALLEMAN, D. & RUDO, D. J. O. D. 2017. Stress-reduced direct composites for the restoration of structurally compromised teeth: Fiber design according to the "wallpapering" technique. 42**,** 233-243.

9- DIKOVA, T., VASILEV, T., HRISTOVA, V. & PANOV, V. 2020. Finite Element Analysis in Setting of Fillings of V-Shaped Tooth Defects Made with Glass-Ionomer Cement and Flowable Composite. 8**,** 363.

10- DIKOVA, T., VASILEV, T., HRISTOVA, V. & PANOV, V. J. J. O. T. M. B. O. B. M. 2021. Finite element analysis of V-shaped tooth defects filled with universal nanohybrid composite using incremental technique. 118**,** 104425.

11- ELRAGGAL, A., ABDELRAHEEM, I. M., WATTS, D. C., ROY, S., DOMMETI, V. K., ALSHABIB, A., ALTHAQAFI, K. A. & AFIFI, R. R. J. D. M. 2024. Biomechanical reinforcement by CAD-CAM materials affects stress distributions of posterior composite bridges: 3D finite element analysis. 40**,** 869-877.

12- ESCOBAR, L. B., PEREIRA DA SILVA, L. & MANARTE-MONTEIRO, P. J. P. 2023. Fracture resistance of Fiber-Reinforced Composite restorations: a systematic review and Meta-analysis. 15**,** 3802.

13- ESKITAŞCıOĞLU, G., BELLI, S. & KALKAN, M. J. J. O. E. 2002. Evaluation of two post core systems using two different methods (fracture strength test and a finite elemental stress analysis). 28**,** 629-633.

14- FAGUNDES, T. C., BARATA, T. J., BRESCIANI, E., SANTIAGO, S. L., FRANCO, E. B., LAURIS, J. R. P. & NAVARRO, M. J. O. D. 2014. Seven-year clinical performance of resin composite versus resin-modified glass ionomer restorations in noncarious cervical lesions. 39**,** 578-587.

15- FERRACANE, J. L. J. D. M. 2011. Resin composite—State of the art. 27**,** 29-38.

16- GAROUSHI, S., GARGOUM, A., VALLITTU, P. K., LASSILA, L. J. J. O. I. & DENTISTRY, C. 2018. Short fiber-reinforced composite restorations: a review of the current literature. 9**,** e12330.

17- GAROUSHI, S., SÄILYNOJA, E., VALLITTU, P. K. & LASSILA, L. J. D. M. 2013. Physical properties and depth of cure of a new short fiber reinforced composite. 29**,** 835-841.

18- HASIJA, M., WADHWA, D., MIGLANI, S., MEENA, B., ANSARI, I. & KOHLI, S. J. E. 2014. Analysis and comparison of stress distribution in class V restoration with different restorative materials using finite element analysis. 26**,** 301-304.

19- HOLLANDERS, A., KUPER, N., HUYSMANS, M. & VERSLUIS, A. J. D. M. 2020. The effect of occlusal loading on cervical gap deformation: A 3D finite element analysis. 36**,** 681-686.

20- ICHIM, I., LI, Q., LOUGHRAN, J., SWAIN, M. & KIESER, J. J. D. M. 2007a. Restoration of non-carious cervical lesions: Part I. Modelling of restorative fracture. 23**,** 1553-1561.

21- ICHIM, I., SCHMIDLIN, P., KIESER, J. & SWAIN, M. J. J. O. D. 2007b.

Mechanical evaluation of cervical glass-ionomer restorations: 3D finite element study. 35**,** 28-35.

22- ISPAS, A., HOLONEC, R., CRIŞAN, T., FODOR, G., CONSTANTINIUC, M. J. H. & MEDICINE, V. 2019. Role of occlusal forces in the development of noncarious cervical lesions. 11**,** 6-10.

23- JAIN, A., SHAH, N. C., KUMAR, M., ISHWAR, S., PURKAYASTHA, D. D., MISHRA, D. & SHANBHAG, A. 2024. Stress distribution pattern in two different no-post systems in endodontically treated maxillary central incisors: A three-dimensional finite element analysis. 27**,** 572-576.

24- JAKUPOVIĆ, S., ŠEHIĆ, A., JULARDŽIJA, F., GAVRANOVIĆ-GLAMOČ, A., SOFIĆ, A., BAJSMAN, A. & KAZAZIĆ, L. J. E. J. O. D. 2022. The Influence of Different Occlusal Loading on Six Restorative Materials for Restoration of Abfraction Lesions—Finite Element Analysis. 16**,** 886-894.

25- JORDEHI, A. Y., SHAHABI, M. S. & AKBARI, A. J. D. R. J. 2019. Comparison of self-adhering flowable composite microleakage with several types of bonding agent in class V cavity restoration. 16**,** 257-263.

26- KHAN, A. A., ZAFAR, M. S., FAREED, M. A., ALMUFAREH, N. A., ALSHEHRI, F., ALSUNBUL, H., LASSILA, L., GAROUSHI, S. & VALLITTU, P. K. J. D. M. 2023. Fiber-reinforced composites in dentistry–An insight into adhesion aspects of the material and the restored tooth construct. 39**,** 141-151.

27- KIM, S.-Y., KIM, B.-S., KIM, H. & CHO, S.-Y. J. D. M. 2021. Occlusal stress distribution and remaining crack propagation of a cracked tooth treated with different materials and designs: 3D finite element analysis. 37**,** 731-740.

28- KUBO, S., KAWASAKI, K., YOKOTA, H. & HAYASHI, Y. J. J. O. D. 2006. Five-year clinical evaluation of two adhesive systems in non-carious cervical lesions. 34**,** 97-105.

29- LASSILA, L., GAROUSHI, S., VALLITTU, P. K. & SÄILYNOJA, E. J. J. O. T. M. B. O. B. M. 2016. Mechanical properties of fiber reinforced restorative composite with two distinguished fiber length distribution. 60**,** 331-338.

30- LASSILA, L., KEULEMANS, F., SÄILYNOJA, E., VALLITTU, P. K. & GAROUSHI, S. J. D. M. 2018. Mechanical properties and fracture behavior of flowable fiber reinforced composite restorations. 34**,** 598-606.

31- LASSILA, L., SÄILYNOJA, E., PRINSSI, R., VALLITTU, P. K. & GAROUSHI, S. J. J. O. T. M. B. O. B. M. 2020. Fracture behavior of Bi-structure fiber-reinforced composite restorations. 101**,** 103444.

32- LEPRINCE, J. G., PALIN, W. M., VANACKER, J., SABBAGH, J., DEVAUX, J. & LELOUP, G. J. J. O. D. 2014. Physico-mechanical characteristics of commercially available bulk-fill composites. 42**,** 993-1000.

33- LUO, X., RONG, Q., LUAN, Q. & YU, X. J. B. O. H. 2022. Effect of partial restorative treatment on stress distributions in non-carious cervical lesions: A three-dimensional finite element analysis. 22**,** 607.

34- MACHADO, A., SOARES, C., REIS, B., BICALHO, A., RAPOSO, L. & SOARES, P. J. O. D. 2017. Stress-strain analysis of premolars with non-carious cervical lesions: Influence of restorative material, loading direction and mechanical fatigue. 42**,** 253-265.

35- MANGOUSH, E., GAROUSHI, S., LASSILA, L., VALLITTU, P. K. & SÄILYNOJA, E. 2021. Effect of Fiber Reinforcement Type on the Performance of Large Posterior Restorations: A Review of In Vitro Studies. 13**,** 3682.

36- NARAYANASWAMY, S., MEENA, N., SHETTY, A., KUMARI, A., NAVEEN, D. J. J. O. C. D. & ENDODONTICS 2008. Finite element analysis of stress concentration in Class V restorations of four groups of restorative materials in mandibular premolar. 11**,** 121-126.

37- REES, J. & JACOBSEN, P. J. J. O. D. 1998. The effect of cuspal flexure on a buccal Class V restoration: a finite element study. 26**,** 361-367.

38- RICHERT, R., FARGES, J.-C., TAMIMI, F., NAOUAR, N., BOISSE, P. & DUCRET, M. J. M. 2020. Validated finite element models of premolars: A scoping review. 13**,** 3280.

39- SAFWAT, E. M., KHATER, A. G., ABD-ELSATAR, A. G. & KHATER, G. A. J. B. O. T. N. R. C. 2021. Glass fiber-reinforced composites in dentistry. 45**,** 190.

40- SCHWENDICKE, F., MÜLLER, A., SEIFERT, T., JEGGLE-ENGBERT, L.-M., PARIS, S. & GÖSTEMEYER, G. J. J. O. D. 2021. Glass hybrid versus composite for non-carious cervical lesions: Survival, restoration quality and costs in randomized controlled trial after 3 years. 110**,** 103689.

41- SOARES, L. M., RAZAGHY, M. & MAGNE, P. J. D. M. 2018. Optimization of large MOD restorations: Composite resin inlays vs. short fiber-reinforced direct restorations. 34**,** 587-597.

42- SOARES, P. V., SANTOS-FILHO, P. C. F., QUEIROZ, E. C., ARAÚJO, T. C., CAMPOS, R. E., ARAÚJO, C. A. & SOARES, C. J. J. J. O. P. 2008. Fracture resistance and stress distribution in endodontically treated maxillary premolars restored with composite resin. 17**,** 114-119.

43- SUZAKI, N., YAMAGUCHI, S., HIROSE, N., TANAKA, R., TAKAHASHI, Y., IMAZATO, S. & HAYASHI, M. J. D. M. 2020. Evaluation of physical properties of fiber-reinforced composite resin. 36**,** 987-996.

45- YAMANEL, K., ÇAGLAR, A., GÜLSAHI, K. & ÖZDEN, U. A. J. D. M. J. 2009. Effects of different ceramic and composite materials on stress distribution in inlay and onlay cavities: 3-D finite element analysis. 28**,** 661-670.

46- YAZICI, A. R., BASEREN, M. & DAYANGAC, B. J. O. D. 2003. The effect of flowable resin composite on microleakage in class V cavities. 28**,** 42-46.

47- ZOTTI, F., FERRARI, F., PAGANELLI, C., PILATI, F., LANZARETTI, G., ARLACCHI, D., ZERMAN, N. J. J. O. C. & DENTISTRY, E. 2024. Increasing the fracture strength of MOD restorations with Ribbond fibers. 707-713.

48- ZOTTI, F., HU, J., ZANGANI, A., ALBANESE, M., PAGANELLI, C. J. J. O. C. & DENTISTRY, E. 2023a. Fracture strength and ribbond fibers: In vitro analysis of mod restorations. 15**,** e318.

49- ZOTTI, F., JIE, H., ZANGANI, A., ALBANESE, M., PAGANELLI, C. J. J. O. C. & DENTISTRY, E. 2023b. Fracture strength and ribbond fibers: In vitro analysis of mod restorations. 15**,** 318-323.

Table 1. Restorative material combinations and thicknesses.

Model restorative material	Adhesive layer	Restorative inner layer	Restorative outer layer	Single
A (GIC)	-	-		-
B (CFC)	50 μm thick	-		-
C	50 μm thick	(SRFC) (~1 mm thick)	(CFC) (1 mm thick)	-
D	50 μm thick	Ribbond layer (~1 mm thick)	(CFC) (1 mm thick)	-

Table 2. Grid independence details.

Mesh type	Size of elements	Stress [MPa]
Course	0.04	~12.58
Medium	0.02	~16.48.
Fine	0.01	~18.92
Extra fine	0.008	~19.83

Table 3. Materials, elastic modulus, and Poisson coefficient.

Material	**Elastic Modulus (GPa)**	**Poisson`s ratio**	**References**
enamel	84	0.33	**(Richert et al., 2020)**
dentin	18.6	0.31	**(Richert et al., 2020)**
Compact bone	13.7	0.3	**(Asmussen et al., 2005)**
Cancellous bone	1.37	0.3	**(Asmussen et al., 2005)**
Periodontal ligament	0.069	0.45	**(Eskitaşcıoğlu et al., 2002)**
GIC (GIC, Fuji II, GC Corp., Tokyo, Japan).	8	0.35	**(Ausiello et al., 2019)**
CFC (3M, Z350, Oral Care, St Paul, MN, USA).	10	0.25	**(Ferracane, 2011)**

Ever x composite (Ever X Posterior from GC, Tokyo, Japan).	12.3	0.22	**(Barreto et al., 2016)**
Ribbond fiber + bonding agent+ Tetric Flow (Ribbond Inc., Seattle WA, USA).	23.6	0.32	**(Eskitaşcıoğlu et al., 2002)**
Adhesive layer (Clearfill SE bond)	3.9	0.32	**(Kim et al., 2021)**

Table 4. Von Mises stress in MPa among different tooth substrates (enamel and dentin), GIC (Model A), CFC (Model B), Ever X-CFC (Model C), and Ribbond-CFC (Model D) during axial loading

Restorative material	Enamel	Dentin	Restoration
GIC	19.8	2.45	0.94
CFC	13.3	1.64	0.66
Ever X-CFC	9.5	0.92	0.24
Ribbond- CFC	6.3	0.57	0.19

Table 5. Von Mises stress in MPa among different tooth substrates (enamel and dentin), GIC (Model A), CFC restoration (Model B), X-CFC (Model C), and Ribbond-PFC (Model D) during oblique loading (45 degrees)

Restorative material	Enamel	Dentin	Restoration
GIC	23.5	3.3	2.75
CFC	17.68	2.94	1.83
Ever X-CFC	9.53	1.36	1.77
Ribbond- CFC	7.8	0.92	2.05

(a) 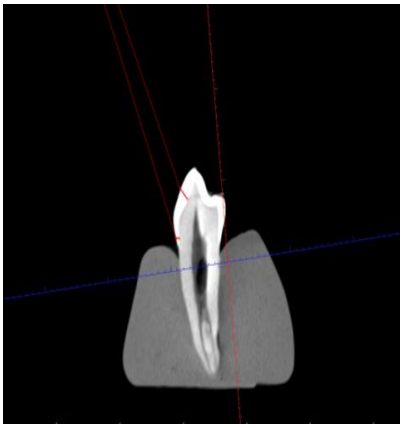 (b) 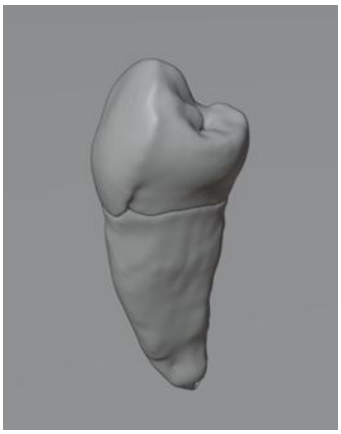

Fig. 1- (a) A sagittal CBCT image of the mandibular first premolar. **(b)** 3D model of the tomographed tooth.

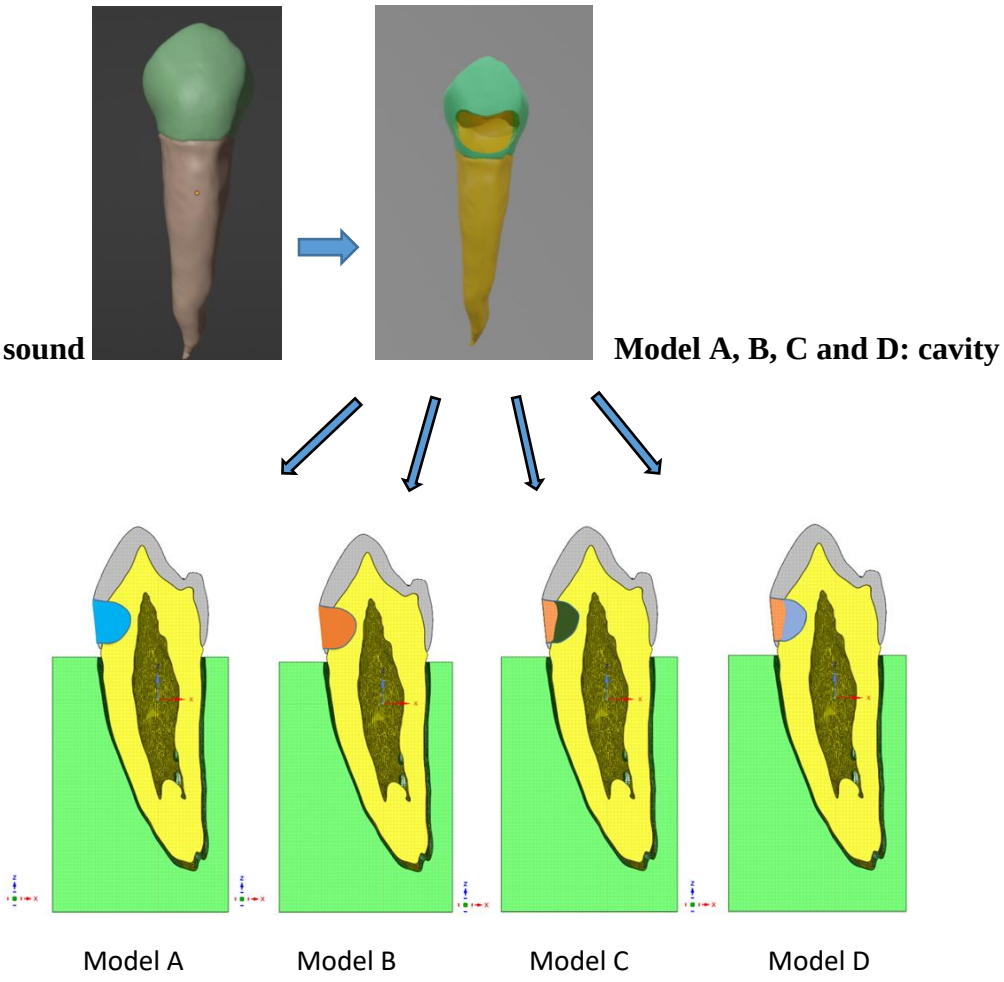

Fig. 2 – Geometric features of the analyzed model.

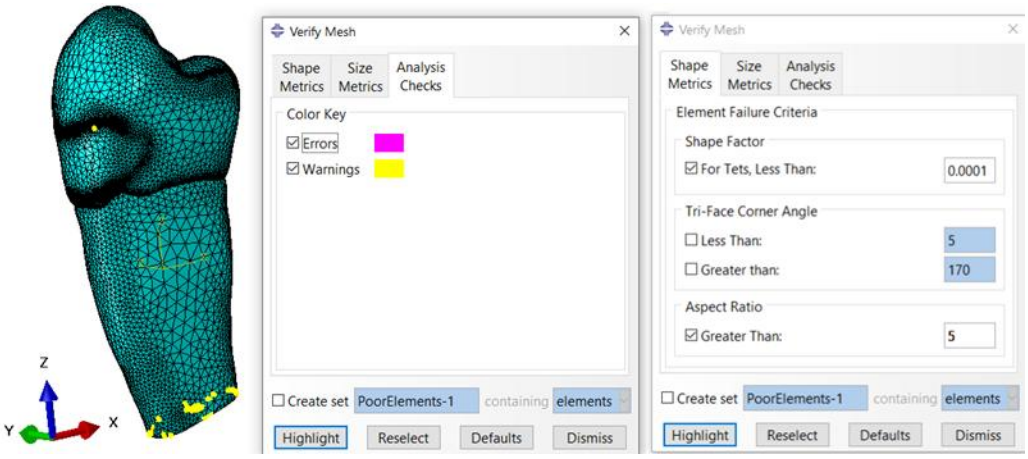

Fig. 3. Mesh quality check of the 3D tooth model: The image shows mesh element warnings based on aspect ratio and shape quality to ensure accuracy and stability in the simulation.

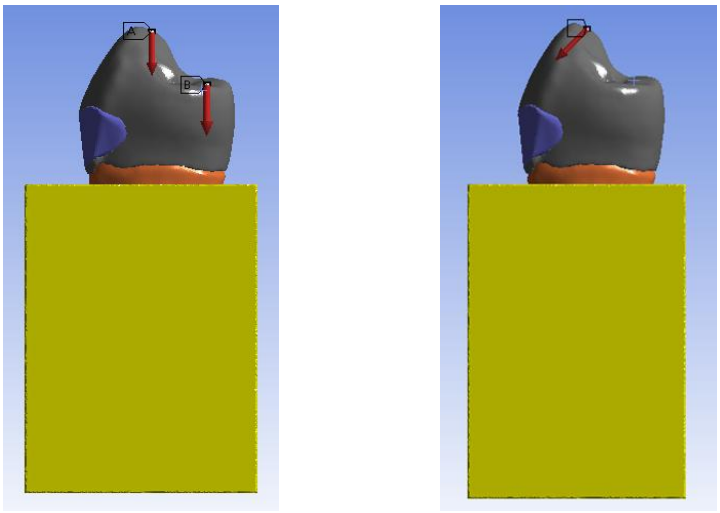

(a) Axial load. (b) Oblique load.

Fig. 4. Types of loading utilized in the study. The same amount of load (150 N) was used for both. Two loading points on the buccal and lingual cusps were used in the case of axial loading, and one point on the lingual incline of the buccal cusp was used in the case of oblique loading.

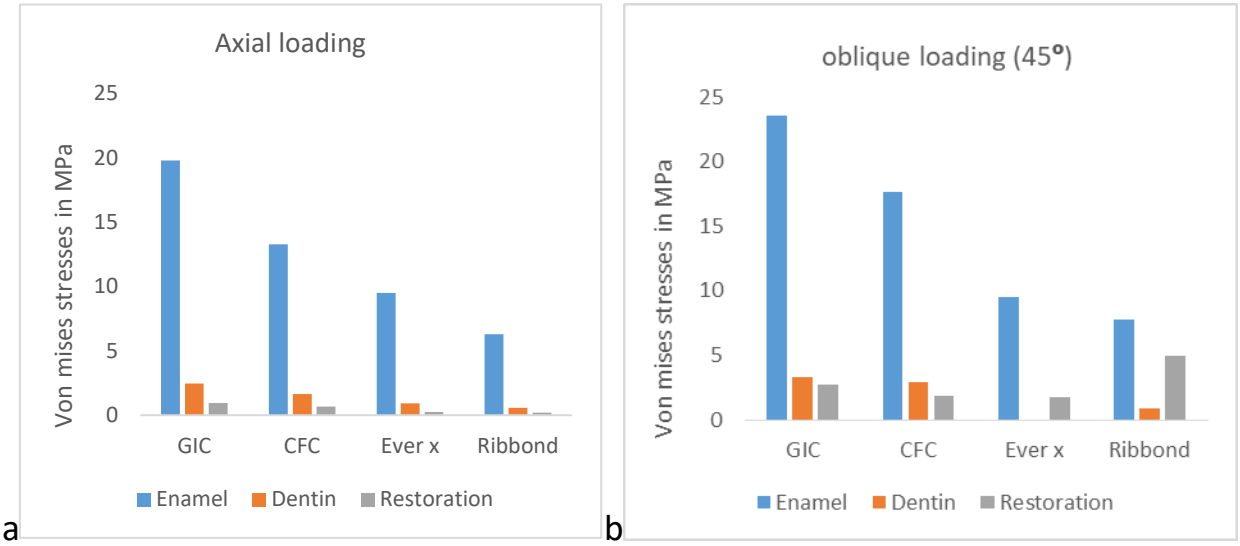

Fig. 5- (a-b). Von mise stress distribution (MPa) for different tooth substrates, GIC, CFC, and bilayered Ever X-CFC, Ribbond-CFC restorations during axial loading (a) and oblique loading (b), as represented in a bar chart.

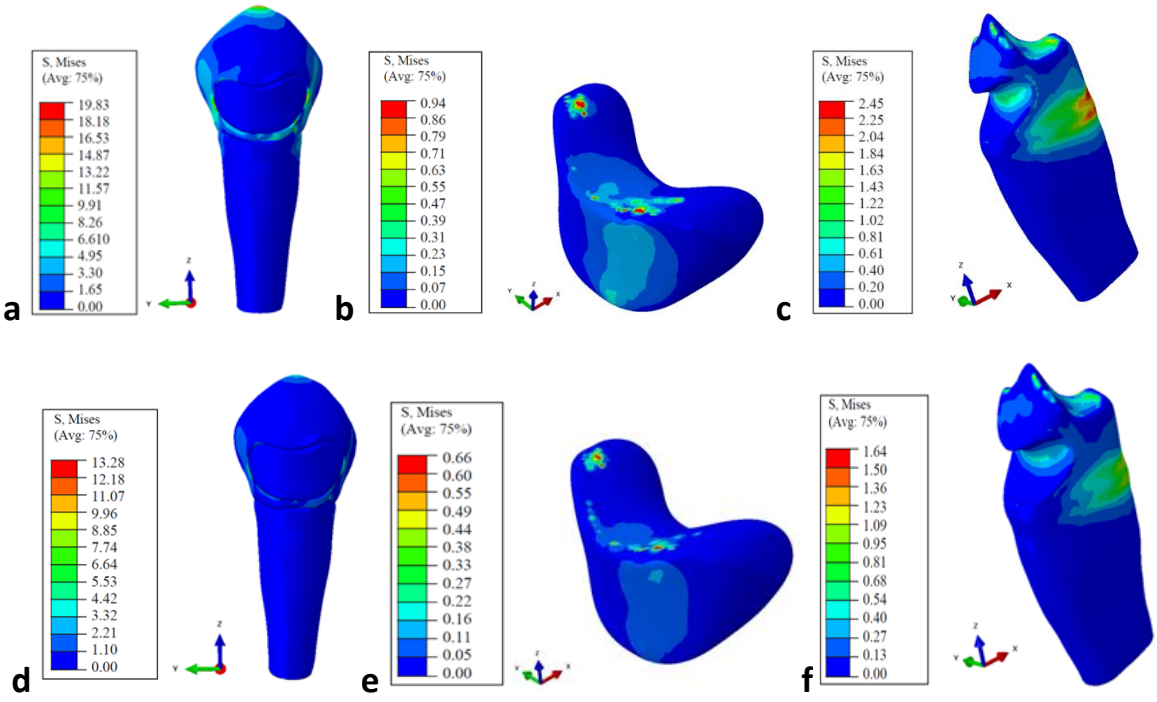

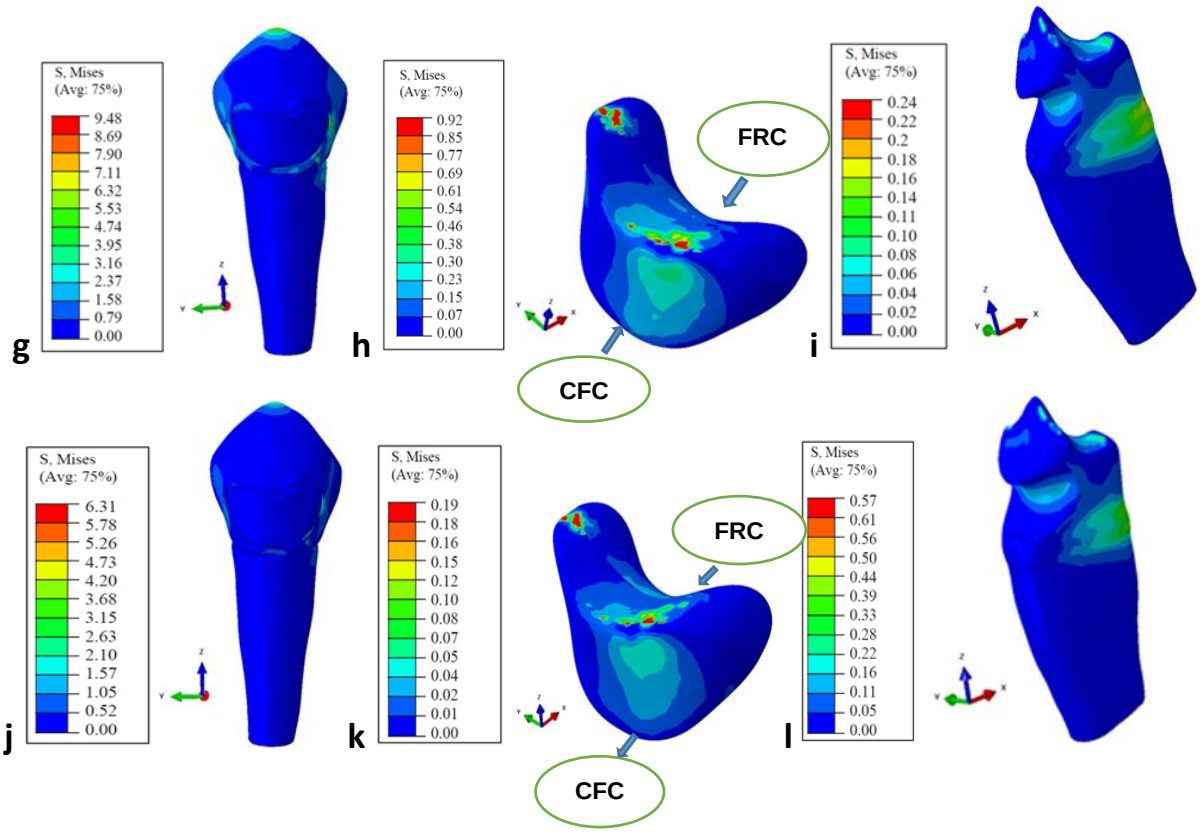

Fig. 6a-l. Von Mises stress distributions during axial loading among different model components (enamel, dentin and restoration), with a-c corresponding to Model A; d-f, Model B; g-i, Model C; and j-l, Model D.

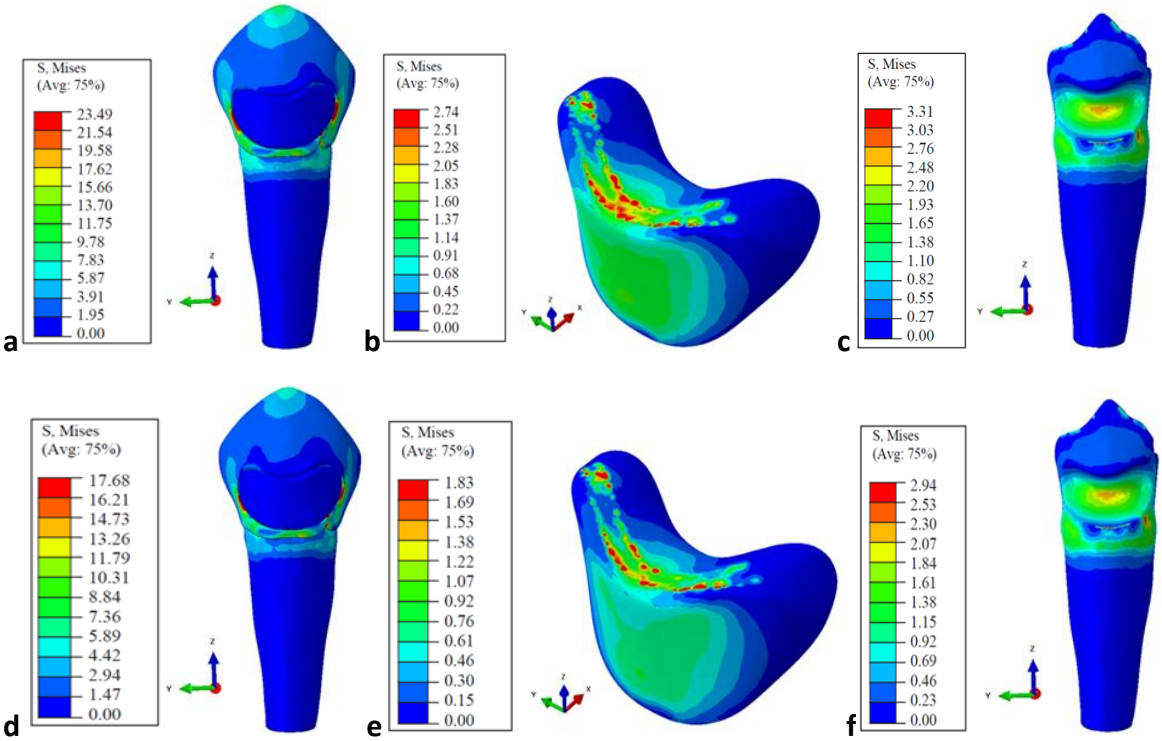

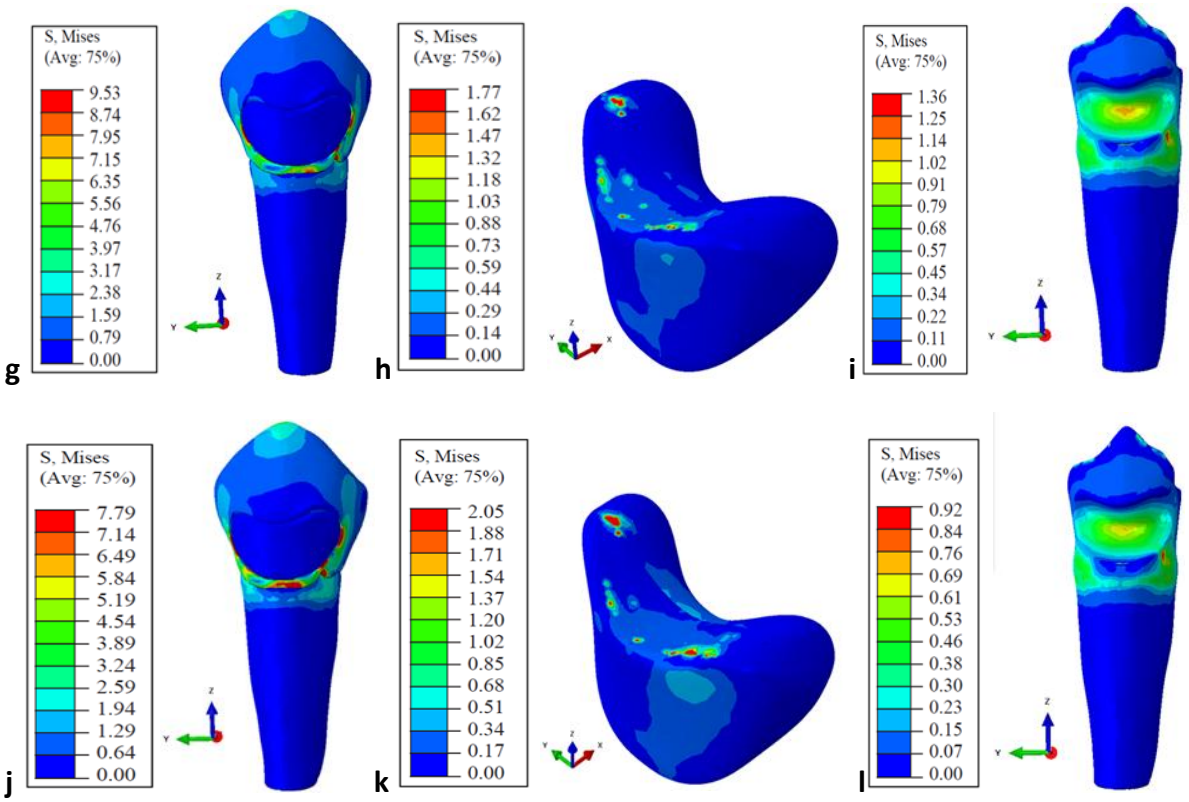

Fig. 7a-l. Von Mises stress distributions during oblique loading among different model components (enamel, dentin and restoration), with a-c corresponding to Model A; d-f, Model B; g-i, Model C; and j-l, Model D.